MECHANICS
МЕХАНИКА

UDC 536.21; 517.958
https://doi.org/10.23947/2687-1653-2026-26-1-2242

Original Theoretical Research

Analytical Solution of the Navier–Stokes Equations for Describing Inhomogeneous Couette Flow with a Quadratic Velocity Profile in a Layer with Permeable Boundaries

EDN: ZWPWMM

Kristina V. Gubareva[1] ✉, **Evgenii Yu. Prosviryakov**[2,3], **Anton V. Eremin**[1]
[1] Samara State Technical University, Samara, Russian Federation
[2] Ural Federal University, Ekaterinburg, Russian Federation
[3] Institute of Engineering Science, RAS (Ural Branch), Ekaterinburg, Russian Federation
✉ r.kristina2017@mail.ru

Abstract

Introduction. Flow control in microfluidic systems, membrane technologies, and porous bearings requires an understanding of the synergy between boundary permeability, their spatial inhomogeneity, and the viscosity of the working fluid. Each of these factors is actively studied separately. However, a comprehensive analytical description of their combined effect on the flow is needed. No such publications exist. The presented article fills this gap. Research objectives are as follows: to obtain an analytical solution for the velocity field in Couette flow with permeable boundaries and a nonlinear boundary condition; to study the formation of hydrodynamics under the influence of permeability (α), dynamic viscosity (μ), linear (A) and quadratic (B) inhomogeneity of the boundary condition.

Materials and Methods. The analytical solution is based on the stationary Navier–Stokes equations for an incompressible Newtonian fluid, with a quadratic expansion of velocity along the transverse coordinate. The axial, linear, and quadratic modes of the velocity profile were investigated using numerical modeling in MATLAB. For a stationary, laminar, isothermal flow of a Newtonian viscous incompressible fluid, the distance between permeable plates was h = 1 m. The lower plate was stationary, while the upper plate moved with a velocity of W = 0.3 m/s. The liquid filtration rate was V_w = 0.001 m/s, and μ = 0.01 Pa·s for $A = \pm 0.03$ s^{-1} and $B = \pm 0.005$ m^{-1}·s^{-1}. Water, motor oil, and crude oil were studied at temperatures of 20 °C, 40 °C, or 60 °C. For this case, h = 0.02 m, W = 0.05 m/s, A = 0.1 s^{-1}, B = 0.02 m^{-1}·s^{-1}, V_w = 0.0005 m/s. Depending on the fluid and temperature, μ ranged from 0.05 to $9.15 \cdot 10^{-3}$ Pa·s.

Results. Asymmetry of the flow, deviation from the channel axis, and variability of the vorticity amplitude ω_y were visualized. Zero filtration velocity was observed at the lower plate in the plane z = 0 and increased with this parameter, reaching a maximum at $z = h$ (distance between the plates). For water, the streamlines exhibited minimal deviation from the horizontal, while for oil at 20 °C, they curved near the upper wall. Two-dimensional vorticity fields for water, oil, and petroleum at various temperatures were compared. Weak ω_y and reduced viscosity resulted in negative values ω_y for water and petroleum. For oil, the situation was reversed: positive values corresponded to elevated ω_y.

Discussion. The calculation results allow us to conclude:

– changing the sign of A inverts the directions of the maxima for velocity and vorticity;

– the sign of B determines the curvature of the isolines;

– the thickness of the layer with the maximum velocity gradient changes by two orders of magnitude when transitioning from water to oil.

The identified patterns are explained by the physical meaning of the parameters: A defines the macroscopic flow asymmetry, B governs the distribution of the transverse flow, and viscosity, through α, controls the depth of boundary perturbations.

Conclusion. For the first time, an exact analytical solution to the stationary Navier–Stokes equations was obtained for generalized Couette flow of a Newtonian fluid between permeable plates with a quadratic velocity profile at the boundary. A parametric analysis has shown that coefficient A determines the asymmetry of the velocity and vorticity fields, while B determines their nonlinearity. Viscosity controls the thickness of the shear layer: for high-viscosity media, the velocity drop is localized near the walls, while for low-viscosity media, the profile is linear. The results provide a foundation for applications in microfluidics, membrane technologies, and tribology. Future prospects are associated with accounting for non-Newtonian fluid properties, unsteady regimes, and flow stability.

Keywords: limitations of the Couette model, hydrodynamic structure of the flow, flow velocity profile, fluid filtration rate, vorticity amplitude, dynamic viscosity

Acknowledgements. The authors would like to thank the Editorial board of the journal and the reviewers for their professional analysis of the article and valuable recommendations for its improvement**.**

For Citation. Gubareva KV, Prosviryakov EYu, Eremin AV. Analytical Solution of the Navier–Stokes Equations for Describing Inhomogeneous Couette Flow with a Quadratic Velocity Profile in a Layer with Permeable Boundaries. *Advanced Engineering Research* (*Rostov-on-Don*). 2026;26(1):2242. https://doi.org/10.23947/2687-1653-2026-26-1-2242

Оригинальное теоретическое исследование

Аналитическое решение уравнений Навье – Стокса для описания неоднородного течения Куэтта с квадратичным профилем в слое с проницаемыми границами

К.В. Губарева[1] ✉, Е.Ю. Просвиряков[2,3], А.В. Еремин[1]

[1] Самарский государственный технический университет, г. Самара, Российская Федерация

[2] Уральский федеральный университет имени первого Президента России Б.Н. Ельцина, г. Екатеринбург, Российская Федерация

[3] Институт машиноведения имени Э.С. Горкунова Уральского отделения Российской академии наук, г. Екатеринбург, Российская Федерация

✉ r.kristina2017@mail.ru

Аннотация

Введение. Управление структурой потока в микрофлюидных системах, мембранных технологиях и пористых подшипниках требует понимания синергии проницаемости границ, их пространственной неоднородности и вязкости рабочей жидкости. Отдельно каждый из этих факторов активно изучается. Однако необходимо комплексное аналитическое описание их совместного влияния на поток. Таких публикаций нет. Представленная статья восполняет этот пробел. Цели работы: получение аналитического решения для поля скорости в течении Куэтта с проницаемыми границами и нелинейным граничным условием; изучение формирования гидродинамики под влиянием проницаемости (α), динамической вязкости (μ), линейной (A) и квадратичной (B) неоднородности граничного условия.

Материалы и методы. Аналитическое решение базируется на стационарных уравнениях Навье – Стокса для несжимаемой ньютоновской жидкости с квадратичным разложением скорости по поперечной координате. Осевую, линейную и квадратичную моды профиля скорости исследовали методом численного моделирования в Matlab. Для стационарного, ламинарного, изотермического течения ньютоновской вязкой и несжимаемой жидкости расстояние между проницаемыми пластинами h = 1 м. Нижняя пластина неподвижна, верхняя движется со скоростью W = 0,3 м/с. Скорость фильтрации жидкости V_w = 0,001 м/с, μ = 0,01 Па·с для A = ±0,03 с$^{-1}$ и B = ±0,005 м$^{-1}$·с$^{-1}$. Воду, моторное масло и нефть исследовали при 20 °С, 40 °С или 60 °С. В этом случае h = 0,02 м, W = 0,05 м/с, A = 0,1 с$^{-1}$, B = 0,02 м$^{-1}$·с$^{-1}$, V_w = 0,0005 м/с. В зависимости от жидкости и температуры μ — от 0,05 до 9,15·10^{-3} Па·с.

Результаты исследования. Визуализированы асимметрия течения, отклонение от оси канала, вариативность амплитуды завихренности ω_y. Нулевая скорость фильтрации отмечается для нижней пластины в плоскости z = 0 и растет с увеличением этого показателя до максимума при $z = h$ (расстояние между пластинами). Для воды линии тока минимально отклоняются от горизонтали, а для масла при 20 °С — искривляются вблизи верхней стенки. Сопоставляются двумерные поля завихренности для воды, масла и нефти при различных температурах. Слабая ω_y и снижение вязкости обусловили отрицательные показатели ω_y для воды и нефти. Для масла ситуация противоположная: положительные показатели при повышенной ω_y.

Обсуждение. Итоги расчетов позволяют утверждать:

– при изменении знака A инвертируются направления смещения максимумов скорости и завихренности;

– знак B определяет кривизну изолиний;

– толщина слоя с максимальным градиентом скорости меняется на два порядка при переходе от воды к маслу.

Выявленные закономерности объясняются физическим смыслом параметров: A задает макроскопическую асимметрию течения, B управляет распределением поперечного потока, а вязкость через α контролирует глубину граничных возмущений.

Заключение. Впервые было получено точное аналитическое решение стационарных уравнений Навье – Стокса для обобщённого течения Куэтта ньютоновской жидкости между проницаемыми пластинами с квадратичным профилем скорости на границе. Параметрический анализ показал, что коэффициент A определяет асимметрию полей скорости и завихренности, а B — их нелинейность. Вязкость контролирует толщину сдвигового слоя: для высоковязких сред перепад скорости локализуется у стенок, для маловязких — профиль линейный. Результаты создают основу для задач микрофлюидики, мембранных технологий и трибологии. Перспективы связаны с учётом неньютоновских свойств жидкости, нестационарных режимов и устойчивости течений.

Ключевые слова: ограниченность модели Куэтта, гидродинамическая структура течения, профиль скорости течения, скорость фильтрации жидкости, амплитуда завихренности, динамическая вязкость

Благодарности. Авторы выражают благодарность редакционной коллегии журнала и рецензенту за профессиональный анализ статьи и рекомендации для ее корректировки.

Для цитирования. Губарева К.В., Просвиряков Е.Ю., Еремин А.В. Аналитическое решение уравнений Навье – Стокса для описания неоднородного течения Куэтта с квадратичным профилем в слое с проницаемыми границами. *Advanced Engineering Research* (*Rostov-on-Don*). 2026;26(1):2242. https://doi.org/10.23947/2687-1653-2026-26-1-2242

Introduction. Precise control of flow structure in thin layers is critically important for modern technologies — from microfluidic devices to lubrication systems. However, in such cases, some classical hydrodynamic models fail to account for a complex set of technological parameters: wide range of working fluid viscosities, wall permeability, as well as their spatial inhomogeneity (roughness, distributed sources) [1]. An example of such an “incomplete” model is the Couette flow between impermeable plates [2]. The presented study is relevant for the advancement of the following applied areas.

1. *Biomedical microfluidics and so-called labs-on-a-chip*. Efficient mixing of reagents or targeted cell delivery require, firstly, fluid injection through porous membranes ($V_w \neq 0$). Secondly, heterogeneous shear flows generated by wall microtopography (modelled by boundary coefficients A and B) are needed [3].

2. *Energy-efficient membrane technologies (desalination, gas separation)*. In this area, performance is determined by the interaction between the longitudinal flow and transverse filtration through a permeable wall, as well as by the viscous properties of the medium being separated [4].

3. *Tribology of porous and textured bearings*. Pressure distribution, friction, and wear directly depend on the lubricant flow in a microscopic gap with complex topography (A, B) and potential filtration (V_w) through a porous liner [5].

The literature analysis made it possible to systematize approaches to describing the aforementioned factors and revealed a significant gap. Both for model [6] and applied problems [7], the effects of boundary permeability determining nonlinear (exponential) velocity profiles is investigated in detail. The effect of complex (including polynomial) boundary conditions on impermeable walls is well described, which is related to problems of stability, heat and mass transfer, and roughness modeling [8]. The effect of rheological properties, including the wide range of viscosities of real fluids, is deeply studied [9]. Modern numerical [10] and analytical [11] methods are actively used to solve conjugate problems. However, the aforementioned factors have been traditionally studied outside of a systems approach. Analytical solutions either describe permeability under homogeneous boundary conditions [12] or account for boundary nonlinearity only for impermeable walls [13]. Thus, the literature lacks a comprehensive analytical solution that explicitly combines the key dimensionless parameters**:**

– dynamic viscosity (μ);

– permeability ($\alpha = \rho V_w/\mu$);

– linear (A) и quadratic (B) corrections to the boundary velocity profile.

It is this gap that prevents a direct parametric analysis of the synergistic influence of the aforementioned factors on the flow structure. Consequently, it is impossible to purposefully design devices for the applied areas listed above.

The objective of this work is to create and analyze an exact solution for generalized stationary Couette flow of a Newtonian fluid between permeable plates with a quadratic velocity profile at the boundary. The scientific novelty lies in obtaining a closed-form analytical solution that, for the first time, explicitly and comprehensively accounts for the synergy of the parameters α, A, B and μ. The primary advantage of this approach over numerical modeling is the ability to obtain a solution instantly and perform a direct analysis of physical dependences, unmediated by grid approximations. To achieve this objective, four tasks are addressed.

1. Output and rigorous verification of the analytical solution, including checking the limiting transitions to known special cases.

2. Investigation of the effect of the sign and magnitude of the boundary coefficients A and B on the spatial distribution of velocity and vorticity.

3. Quantitative analysis of the effect of the dynamic viscosity of real fluids (water, engine oil, petroleum) on the velocity profile and shear layer thickness.

4. Discussion of the practical significance of the results, model limitations, and promising directions for the model generalization.

Materials and Methods. Let us consider a steady (stationary), laminar, isothermal flow of a Newtonian viscous and incompressible fluid in a channel formed by two infinite, parallel, flat plates (Fig. 1).

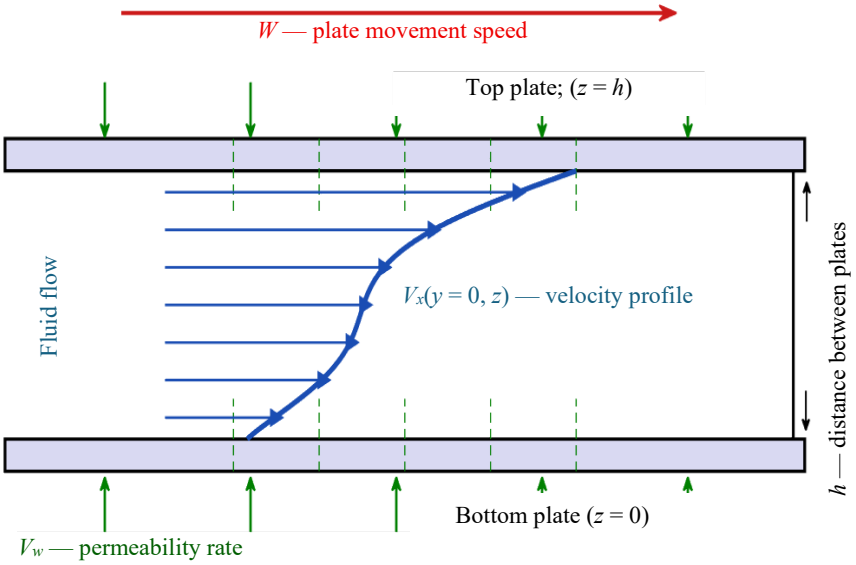

Fig. 1. Schematic diagram of Couette flow between permeable plates

The distance between the plates is constant and equal to h. The bottom plate is stationary and located in the plane $z = 0$. The top plate is located in the plane $z = h$ and moves with constant velocity W in the positive x direction.

A key feature of this problem is the permeability of both plates, which enables fluid filtration in the direction normal to their surfaces [6]. It is assumed that this normal velocity (V_w) is constant over the entire surface of each plate and is the same for both plates. If $V_w > 0$, fluid enters the channel through the bottom plate and exits through the top plate; if $V_w < 0$, the flow direction through the walls is reversed.

The longitudinal velocity component V_x is specified as a quadratic expansion in the transverse coordinate y. This generalization of the classical Couette profile allows for more complex boundary conditions on the top plate [5]:

$$V_x(y,z) = U(z) + yu_1(z) + \frac{y^2}{2}u_2(z). \quad (1)$$

Here, functions $U(z)$, $u_1(z)$ and $u_2(z)$ represent the primary (axial), linear, and quadratic modes of the velocity profile, respectively, depending only on the coordinate z.

Boundary conditions are formulated on the basis of the no-slip condition. On the stationary bottom plate ($z = 0$), a complete absence of motion is specified:

$$U(0) = 0,\ u_1(0) = 0,\ u_2(0) = 0. \quad (2)$$

On the top plate ($z = h$), a generalized velocity profile is specified:

$$U(h) = W,\ u_1(h) = A,\ u_2(h) = B, \quad (3)$$

where W — rate of translational motion of the plate; A — coefficient determining the linear velocity gradient along y; B — coefficient determining the profile curvature.

Unknown functions $U(z)$, $u_1(z)$ and $u_2(z)$ can be found from the Navier–Stokes equation for the x-component of velocity. Under the assumption of stationarity, it takes the form [2]:

$$\rho\left(V_x\frac{\partial V_x}{\partial x}\middle|V_y\frac{\partial V_x}{\partial y}\middle|V_z\frac{\partial V_x}{\partial z}\right) = -\frac{\partial p}{\partial x} + \mu\left(\frac{\partial^2 V_x}{\partial x^2}\middle|\frac{\partial^2 V_x}{\partial y^2}\middle|\frac{\partial^2 V_x}{\partial z^2}\right). \quad (4)$$

The flow under consideration is a generalization of pure Couette flow, which is characterized by the absence of a pressure gradient along the channel ($\partial p/\partial x = 0$). Taking this condition into account, as well as the facts that V_x is independent of x, $V_y = 0$ and $V_z = V_w = const$ [3]. In this case, equation (4) is simplified significantly:

$$\rho V_w \frac{\partial V_x}{\partial z} = \mu\left(\frac{\partial^2 V_x}{\partial y^2} | \frac{\partial^2 V_x}{\partial z^2}\right). \tag{5}$$

Substituting (1) into (5) and computing the corresponding derivatives yields an equation that must hold for all values of y. Equating coefficients of like powers of y gives a system of three independent ordinary differential equations (ODE) [11]:

$$\mu u_1'' - \rho V_w u_1' = 0, \tag{6}$$

$$u_2'' - \rho V_w u_2' = 0, \tag{7}$$

$$\mu U'' - \rho V_w U' = -\mu u_2. \tag{8}$$

Expressions (6) and (7) are second-order linear homogeneous ordinary differential equations (ODE) with constant coefficients. To solve them, the dimensionless permeability parameter $\alpha = \rho V_w / \mu$ is introduced, which physically represents the ratio of inertial forces to viscous forces in the normal direction. Dividing (6) and (7) by μ gives the canonical form:

$$u_1'' - \alpha u_1' = 0, \quad u_2'' - \alpha u_2' = 0. \tag{9}$$

The general solutions to these equations are:

$$u_1(z) = C_1^{(1)} + C_2^{(1)} e^{\alpha z}, \quad u_2(z) = C_1^{(2)} + C_2^{(2)} e^{\alpha z}. \tag{10}$$

Using boundary conditions (2) and (3) allows us to determine the integration constants. For function $u_1(z)$, the conditions $u_1(0) = 0$ and $u_1(h) = A$ yield:

$$C_1^{(1)} = -C_2^{(1)}, \quad C_2^{(1)} = \frac{A}{e^{\alpha h} - 1}. \tag{11}$$

Similarly, for $u_2(z)$ from the conditions $u_2(0) = 0$ and $u_2(h) = B$, we find:

$$C_1^{(2)} = -C_2^{(2)}, \quad C_2^{(2)} = \frac{B}{e^{\alpha h} - 1}. \tag{12}$$

Final expressions for the linear and quadratic modes of the velocity profile:

$$u_1(z) = \frac{A}{e^{\alpha h} - 1}\left(e^{\alpha z} | 1\right), \tag{13}$$

$$u_2(z) = \frac{B}{e^{\alpha h} - 1}\left(e^{\alpha z} | 1\right). \tag{14}$$

Equation (8) for the fundamental mode $U(z)$ is inhomogeneous. We substitute into it the expression found for $u_2(z)$ (14) and divide by μ:

$$U'' - \alpha U' = -\frac{B}{e^{\alpha h} - 1}\left(e^{\alpha z} | 1\right). \tag{15}$$

For equation (15), the method of undetermined coefficients [13] is applied. Its general solution is the sum of the general solution to the homogeneous equation and a particular solution to the non-homogeneous equation. After determining the constants of integration from the boundary conditions (2) and (3), the final expression for the primary mode takes the form [14]:

$$U(z) = \left[\frac{W}{e^{\alpha h} - 1} | \frac{Bh\left(e^{\alpha h} + 1\right)}{\alpha\left(e^{\alpha h} - 1\right)^2}\right]\left(e^{\alpha z} | 1\right) - \frac{B}{\alpha\left(e^{\alpha h} - 1\right)} z\left(e^{\alpha z} | 1\right). \tag{16}$$

Thus, substituting (13), (14), and (16) into the original ansatz (1) yields the full field of the longitudinal velocity component. The analytical solution obtained satisfies both the equation of motion (5) and all boundary conditions, i.e., (2) and (3).

To confirm the physical validity of the solution, let us consider the limiting transition $V_w \to 0$, which is equivalent to $\alpha \to 0$. In this limit, using the Taylor series expansion of the exponential, we obtain for the quadratic mode:

$$u_2(z) \to \frac{Bz}{h}, \quad \alpha \to 0. \tag{17}$$

Similarly for the linear mode:

$$u_1(z) \to \frac{Az}{h}, \quad \alpha \to 0. \tag{18}$$

For the fundamental mode:

$$(z) \to \frac{Wz}{h} + \frac{B}{6h}\left(h^2 z \mid z^3\right), \quad \alpha \to 0. \tag{19}$$

Numerical modeling. At this stage, the following is performed:

– verification and analysis of the obtained solution;

– investigation of the effect of physical parameters on the flow structure.

To this end, the authors of the presented article conducted comprehensive numerical modeling in the MATLAB environment. The primary objectives of the software implementation were:

– visual representation of velocity fields;

– quantitative comparison of flow characteristics for various fluid types and boundary conditions.

The central element of the code is *solve_couette_full* function, which implements formulas (13), (14), and (16).

The inputs are:

– physical properties of the fluid (density ρ and dynamic viscosity μ);

– geometric parameters of the problem (distance between the plates h);

– kinematic characteristics (W, A, B, V_w);

– z-coordinate grid.

The output is the basic functions $U(z)$, $u_1(z)$, $u_2(z)$ and their derivatives with respect to z for the subsequent calculation of such important hydrodynamic quantities as shear stress and vorticity.

The modeling was conducted in two stages. In the first stage, a basic calculation was performed for a standard set of parameters. This allowed for verification of the boundary conditions. The maximum deviation of the velocity from the specified values at the boundaries $z = 0$ and $z = h$ did not exceed 10^{-12}, which confirmed the high accuracy of the analytical approach and the correctness of the software implementation.

In the second stage, the code was extended to analyze two key aspects. First, the effect of the signs and magnitudes of the coefficients A and B in the boundary velocity profile on the top plate was investigated in detail. Four combinations were considered: $A > 0$, $B > 0$; $A > 0$, $B < 0$; $A < 0$, $B > 0$; $A < 0$, $B < 0$. This allowed for the simulation of several physical scenarios (from flow acceleration toward the channel center to its deceleration near the walls), as well as the transition from convex to concave velocity profiles. For each combination, two-dimensional maps of the velocity distribution $V_x(y, z)$ and velocity profiles along the normal to the plates at fixed values of the transverse coordinate y were constructed. This provided a clear visual representation of how changing the sign of the quadratic term B altered drastically the shape of the velocity isolines, and how the sign of the linear coefficient A determined the asymmetry of the profile relative to the plane $y = 0$.

Secondly, the flow for various fluids was calculated. The model incorporated the physical properties of water SAE 30[1] engine oil, and petroleum at temperatures of 20°C, 40°C, or 60°C [14]. The use of reference data for dynamic viscosity and density made it possible to move from an abstract mathematical model to practically significant engineering calculations. For each fluid, the Reynolds number $Re=Wh/\nu$ was automatically determined, which made it possible to assess the flow regime. As expected, for water at room temperature, the Reynolds number reached $Re\approx1000$. At the same time, the flow remained laminar, which was consistent with the known stability of classical Couette flow. For oil and petroleum, the flow remained deeply laminar ($Re < 20$).

Particular attention was paid to the calculation of derived quantities. For each value of the coordinate y, the shear stress $\tau_{xz} = \mu\partial V_x/\partial z$ and the vorticity $\omega_y = -\partial V_x/\partial z$ were computed analytically. This made it possible to avoid errors of numerical differentiation [15] and ensured high accuracy in constructing the distributions of the specified quantities both along the gap between the plates and as a function of the transverse coordinate y.

Thus, the program developed in MATLAB is a tool for the comprehensive analysis of generalized Couette flow. It can be used to:

– verify the correctness of the analytical solution;

– conduct an in-depth study of the effect of the physical properties of the working medium and complex boundary conditions on the flow hydrodynamics;

– obtain extensive visual and quantitative data for further analysis.

[1] From the name of the American organization Society of Automotive Engineers — Association of Automotive Engineers.

Functions $u_1(z)$, $u_2(z)$, $U(z)$ were parametrically investigated using the numerical modeling method in MATLAB based on the analytical solution derived from (13), (14), and (16). The calculations were performed with the following fixed parameters (Figs. 2–5): $h = 1.0$ m, $W = 0.3$ m/s, $V_w = 0.001$ m/s, $\mu = 0.01$ Pa·s, for four combinations of signs: $A = \pm 0.03$ s^{-1} and $B = \pm 0.005$ m^{-1}·s^{-1}.

For real fluids, calculations were performed with $h = 0.02$ m, $W = 0.05$ m/s, $A = 0.1$ s^{-1}, $B = 0.02$ m^{-1}·s^{-1}, $V_w = 0.0005$ m/s. The following were used: water at 20°C ($\mu = 1.002 \cdot 10^{-3}$ Pa·s) and 40°C ($\mu = 0.653 \cdot 10^{-3}$ Pa·s); petroleum at 20°C ($\mu = 9.15 \cdot 10^{-3}$ Pa·s) and 40°C ($\mu = 4.72 \cdot 10^{-3}$ Pa·s);); SAE 30 oil at 20°C ($\mu = 0.290$ Pa·s) and 60°C ($\mu = 0.050$ Pa·s).

Research Results. Figure 2 shows the vorticity fields ω_y. For $A > 0$, the maximum positive values ω_y are located in the region of positive coordinates y. For $A < 0$, maxima ω_y are shifted to the region $y < 0$. The amplitude of the values ω_y varies with changes in coefficient B.

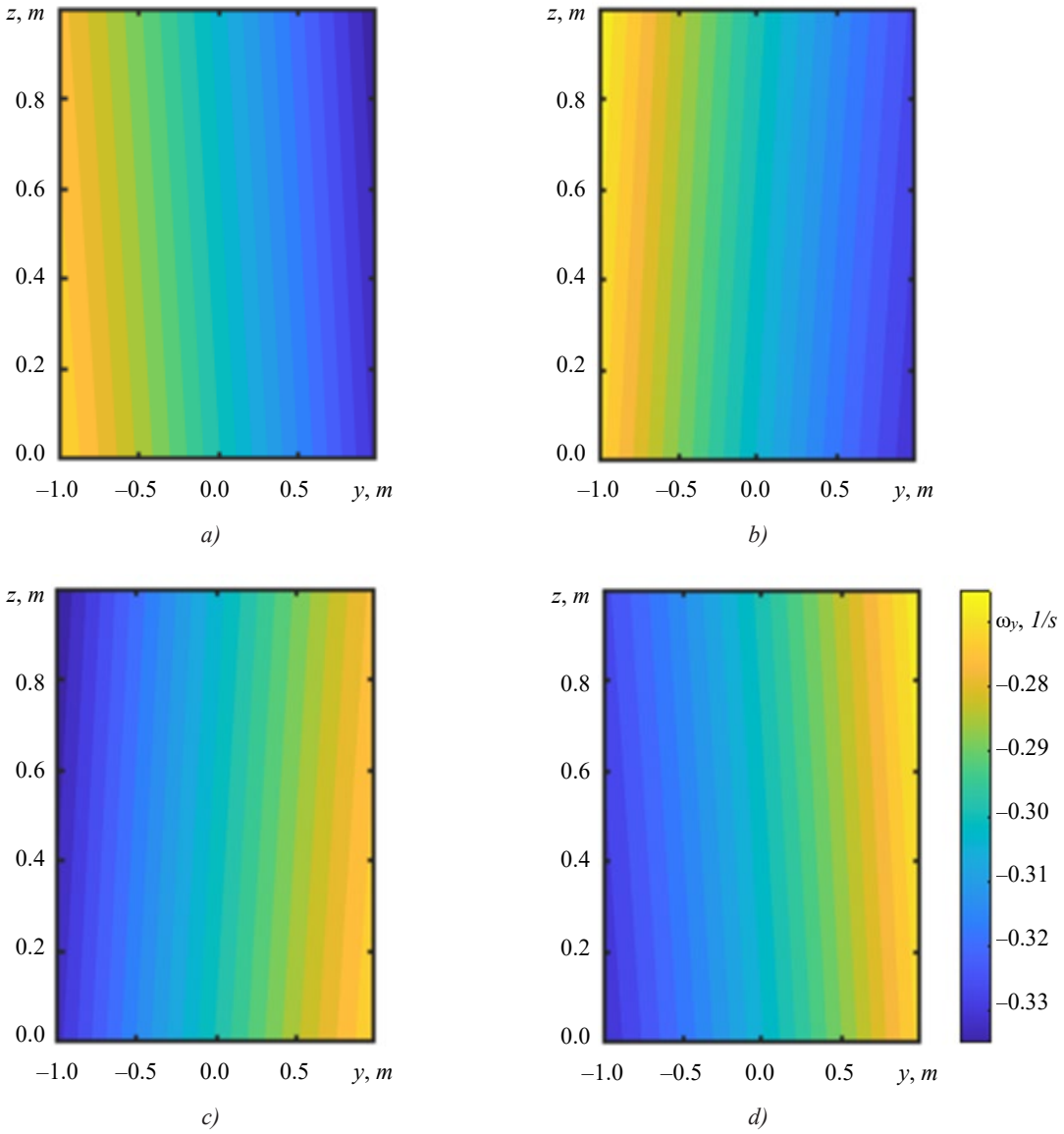

Fig. 2. Distribution of vorticity ω_y for different combinations of parameter signs A and B:
a — $A > 0$, $B > 0$; *b* — $A > 0$, $B < 0$; *c*— $A < 0$, $B > 0$; *d* — $A < 0$, $B < 0$

Figure 3 shows the velocity magnitude field $|V|$ and the vector field for two combinations of the signs of parameters A and B. For $A > 0$, the vectors are longer in the region $y > 0$, indicating a shift of the velocity maximum towards the positive transverse coordinate region. For $A < 0$, the opposite pattern is observed: the vectors are longer in the region $y < 0$, which indicates a shift of the maximum towards the negative region. This is a manifestation of flow asymmetry caused by the linear term A in the boundary condition. The shape of isolines $|V|$ differs for the cases $B > 0$ and $B < 0$, which is related to the effect of the quadratic term B.

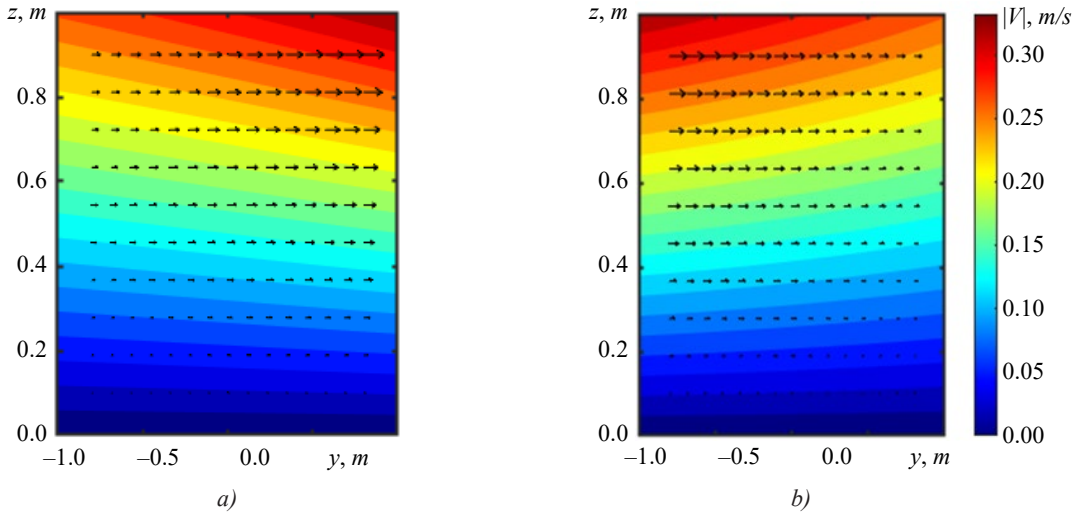

Fig. 3. Velocity modulus field and vector field for different combinations of parameter signs A and B:
a — $A > 0$, $B > 0$; $A > 0$, $B < 0$; b — $A < 0$, $B > 0$; $A < 0$, $B < 0$

Figure 4 presents the isolines of the longitudinal velocity V_x and the streamlines. The streamlines deviate from the direction of the channel axis. The direction of the deviation is determined by the sign A. The isolines V_x for $B > 0$ and $B < 0$ have different curvatures.

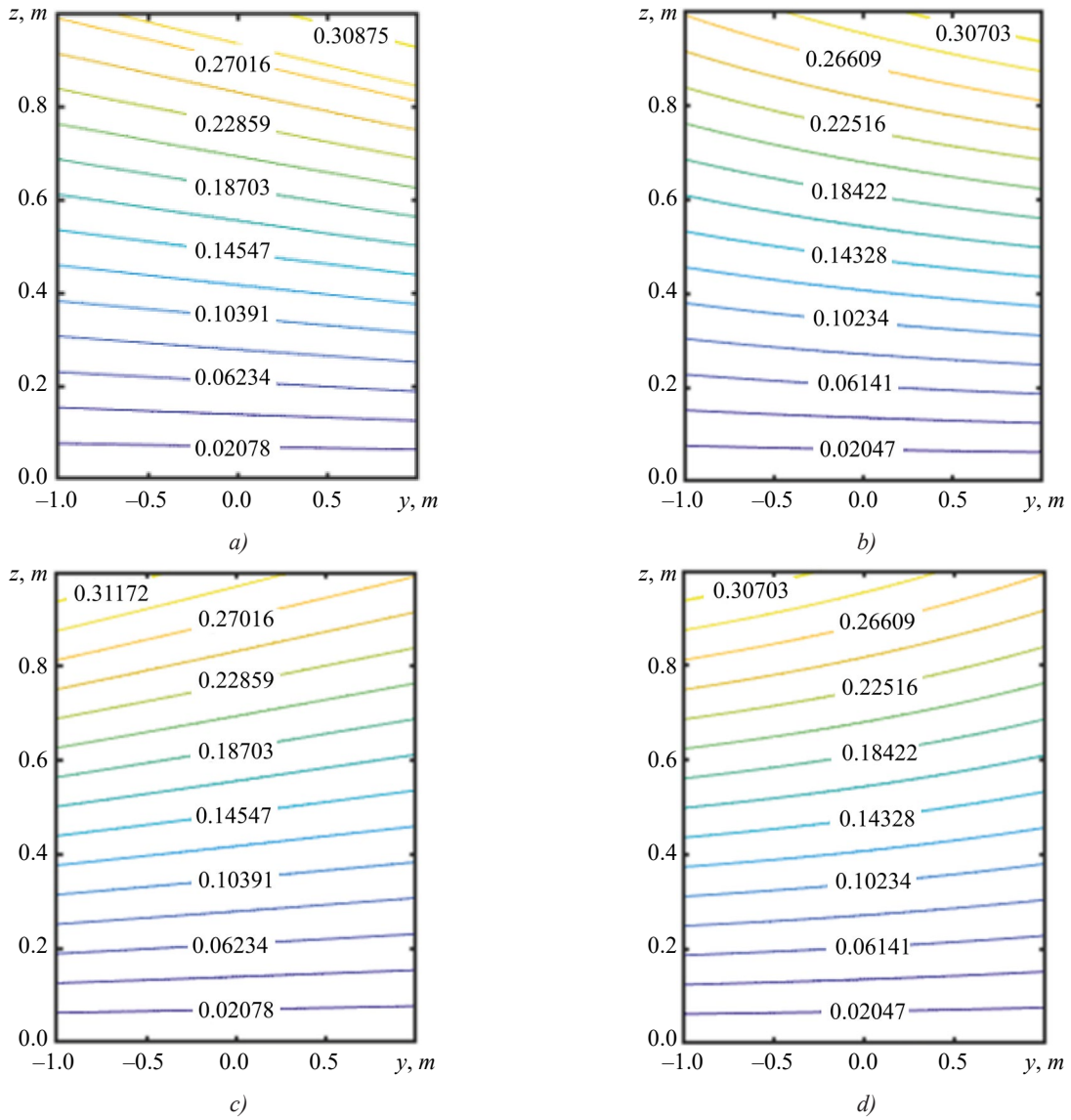

Fig. 4. Isolines of the velocity component V_x and streamlines for different combinations of parameter signs A and B:
a — $A > 0$, $B > 0$; b — $A > 0$, $B < 0$; c — $A < 0$, $B > 0$; d — $A < 0$, $B < 0$

Figure 5 shows the profiles $V_x(y)$ at different levels, i.e., at $z = 0$, h, $h/4$, $h/2$ and $3h/4$. At $z = 0$, the velocity V_x is zero. As z increases, the variation V_x with y increases and reaches the maximum at $z = h$, where the profile is determined by parameters A and B. At $z = h/2$, the profile is close to linear.

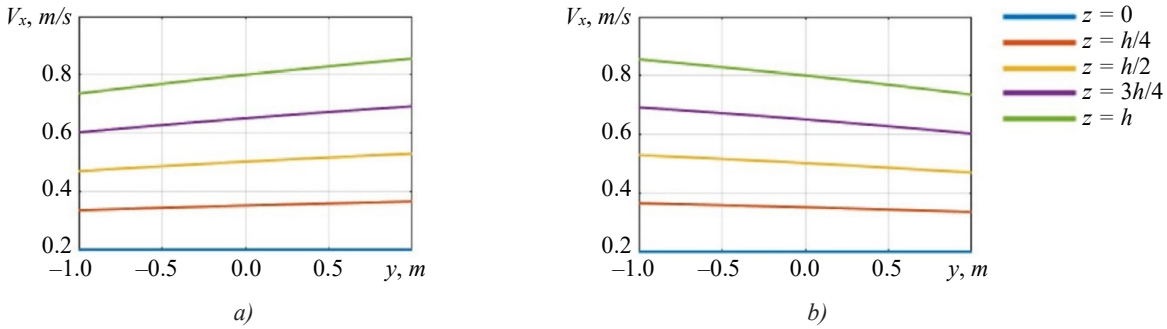

Fig. 5. Distribution of the velocity component V_x along the transverse coordinate y at different channel height levels:

a — $A > 0$, $B > 0$; $A > 0$, $B < 0$; b — $A < 0$, $B > 0$; $A < 0$, $B < 0$

The calculations were performed for real fluids with $h = 0.02$ m, $W = 0.05$ m/s, $A = 0.1$ s^{-1}, $B = 0.02$ m^{-1}·s^{-1}, $V_w = 0.0005$ m/s (Figs. 6–8). The following were used: water at 20°C ($\mu = 1.002 \cdot 10^{-3}$ Pa·s) and 40°C ($\mu = 0.653 \cdot 10^{-3}$ Pa·s); petroleum at 20°C ($\mu = 9.15 \cdot 10^{-3}$ Pa·s) and 40°C ($\mu = 4.72 \cdot 10^{-3}$ Pa·s); SAE 30 oil at 20°C ($\mu = 0.290$ Pa·s) and 60°C ($\mu = 0.050$ Pa·s).

Figure 6 shows the profiles $V_x(z)$ at $y = 0$. All profiles are plotted within the range $z \in [0, 20]$ mm, which corresponds to the layer thickness.

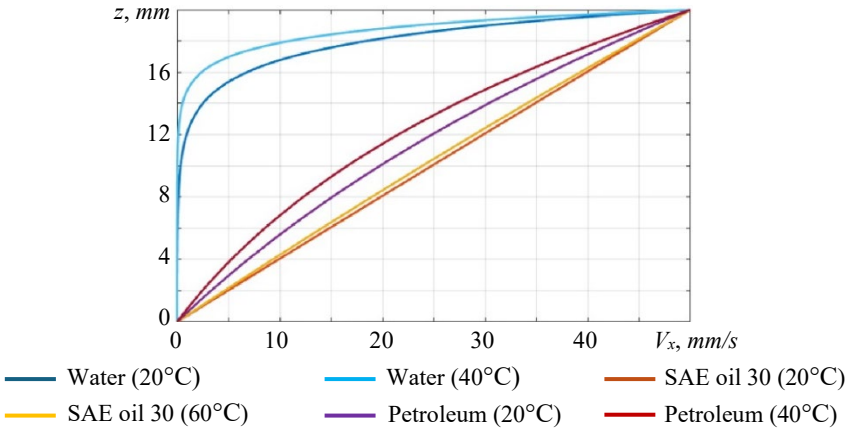

Fig. 6. Comparison of velocity profiles V_x(z) at $y = 0$ for various fluids

Figure 7 displays the isolines $|V|$ For water, the streamlines show minimal deviation from the horizontal, while for petroleum at 20°C, they are significantly curved near the upper wall.

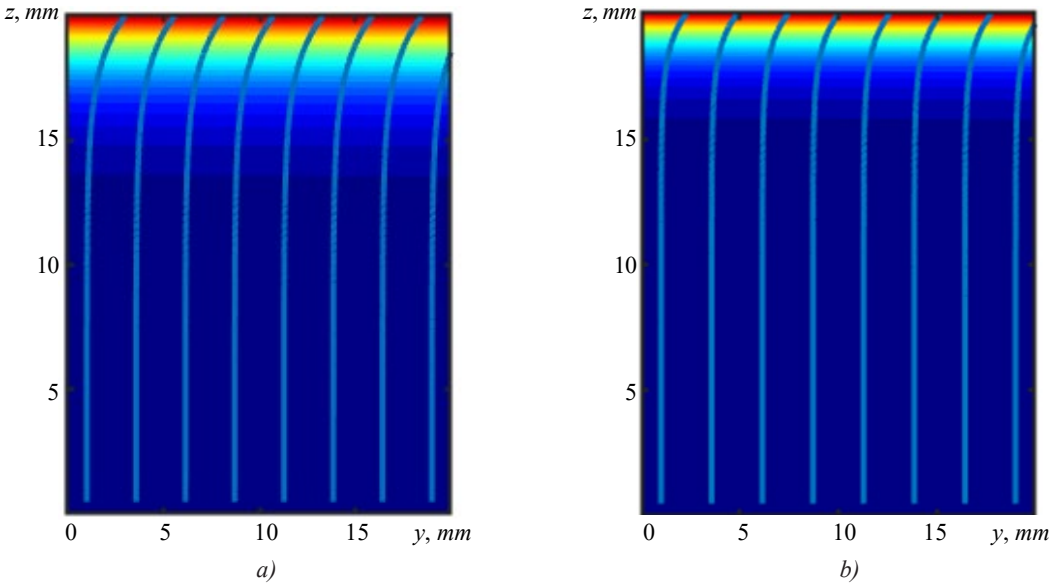

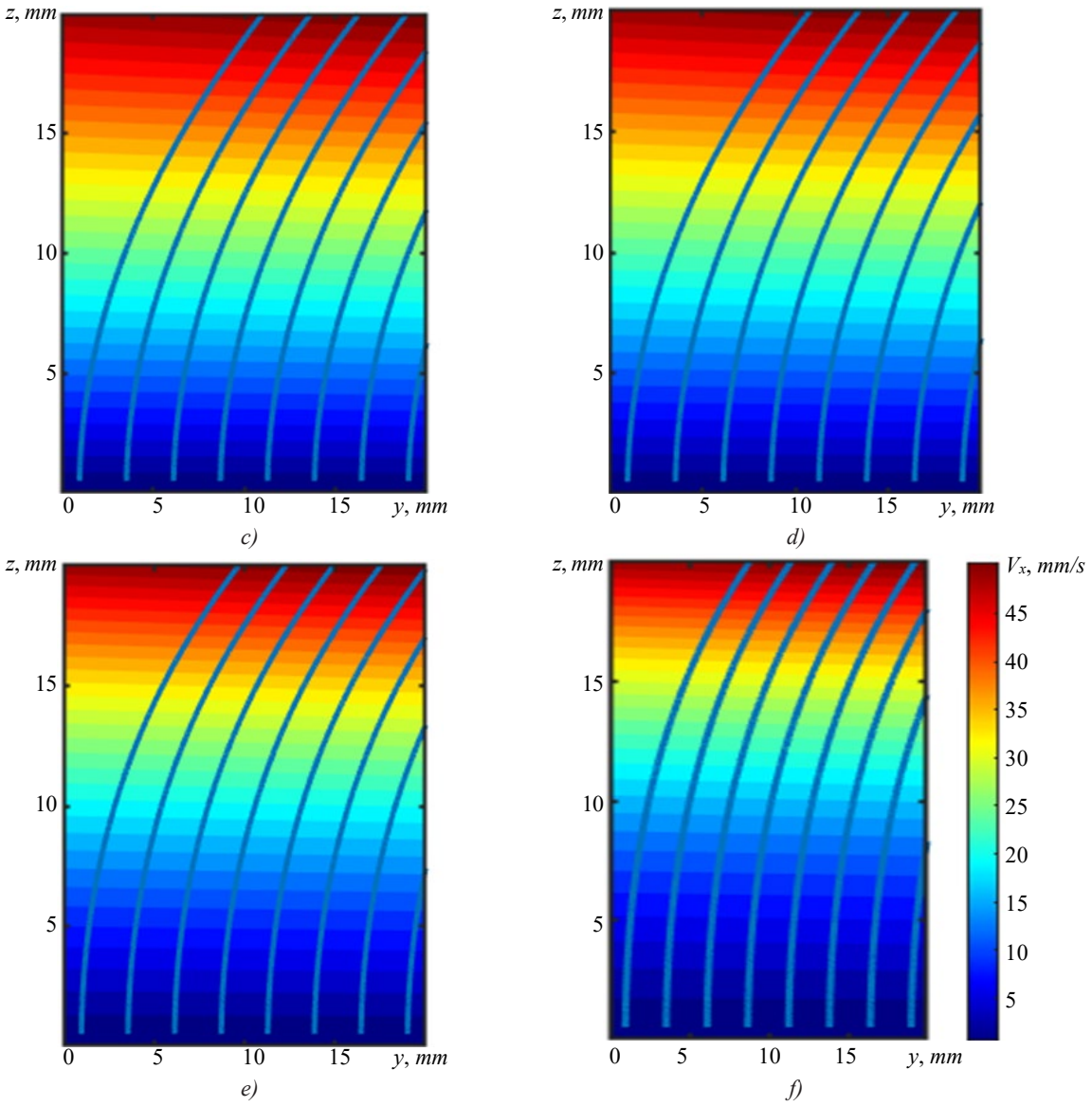

Fig. 7. Isolines of the velocity module $|\vec{V}|$ and streamlines for various fluids:
a — water (20°C); *b* — water (40°C); *c* —SAE oil (20°C); *d* — SAE oil (60°C);
e — petroleum (20°C); *f* — petroleum (40°C)

Figure 8 shows two-dimensional vorticity fields ω_y for various fluids.

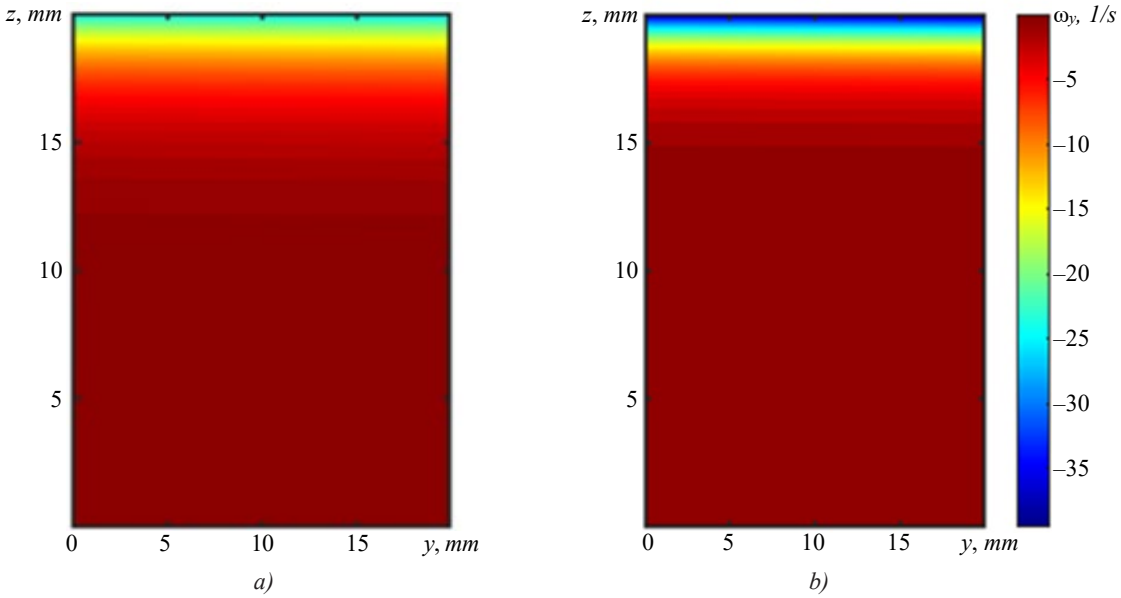

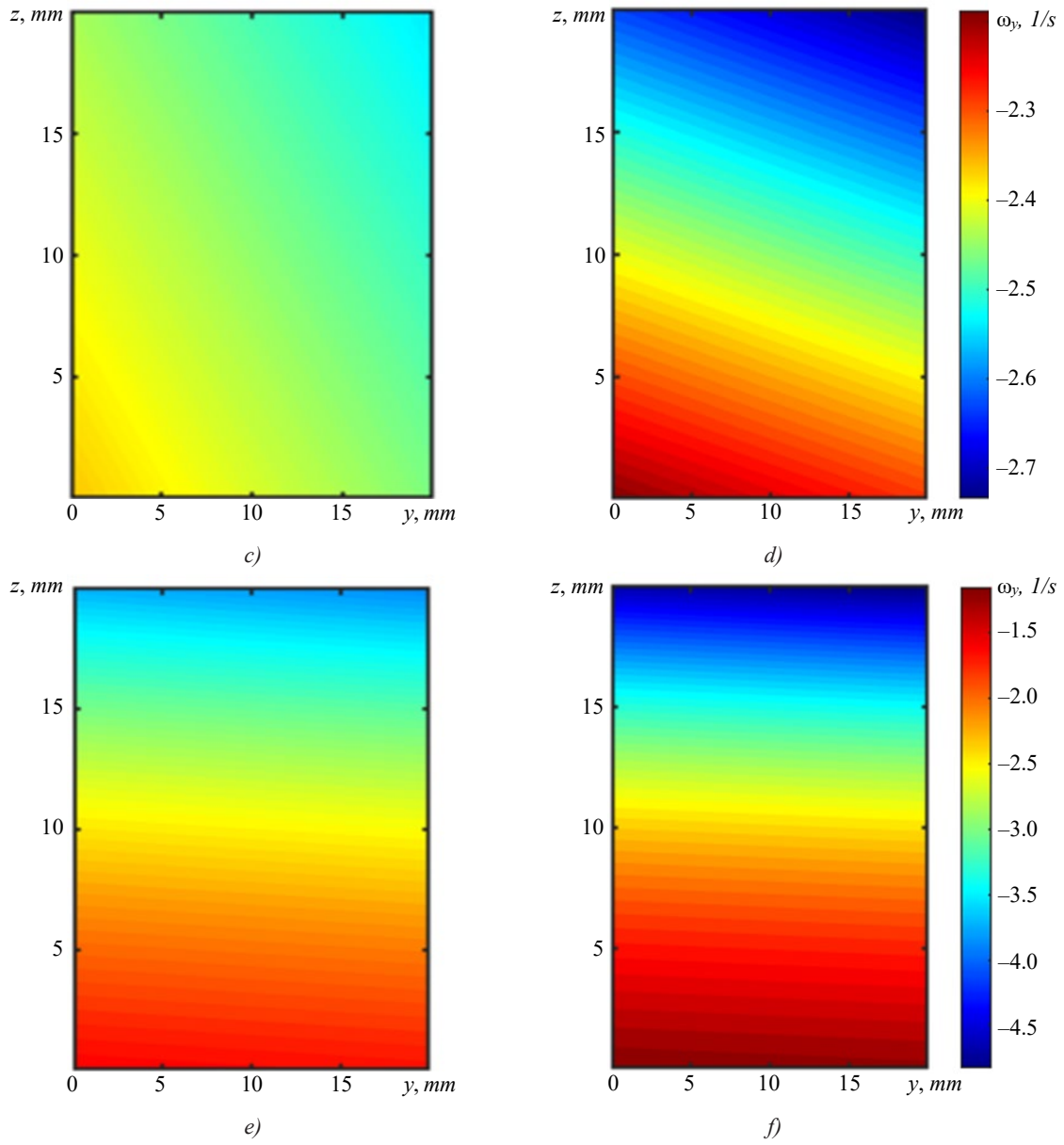

Fig. 8. Two-dimensional vorticity fields ω_y for various fluids: *a* — water (20°C); *b* — water (40°C); *c* — SAE oil (20°C); *d* — SAE oil (60°C); *e* — petroleum (20°C); *f* — petroleum (40°C)

Discussion. According to the data in Figure 6, for water at 20°C, the profile $V_x(z)$ exhibits a weak deviation from the linear law, which is associated with its low viscosity. When the temperature increases to 40°C, this deviation becomes even less pronounced, and the overall slope of the profile slightly decreases. For SAE 30 oil (20°C), a moderate non-linearity of the profile is observed, which weakens significantly upon heating to 60°C. In this case, the profile approaches the linear one, which corresponds to a decrease in viscosity with increasing temperature. For petroleum (20°C), the profile is characterized by a pronounced non-linearity. When the temperature increases to 40°C, the curve becomes closer to the linear one, which is also consistent with a decrease in viscosity.

As shown in Figure 8, for water at 20°C and 40°C, the vorticity is negative and varies in the range from –35 to –5 s^{-1}, which corresponds to weak vorticity throughout the channel. For SAE 30 oil at 20°C, a localized region of elevated vorticity magnitude ($|\omega_y| > 2{,}3$ c^{-1}), is observed, concentrated near the upper wall. Upon heating to 60°C, the region of elevated vorticity expands, and its magnitude decreases, which is consistent with the reduction in viscosity. For petroleum at 20°C, vorticity reaches values up to –4.5 s^{-1}, and at 40°C up to –1.5 s^{-1}, which also corresponds to a decrease in viscosity.

The research results allow us to assert that the combined action of permeability, nonlinear boundary conditions and viscosity, determines qualitatively new flow regimes that cannot be reduced to a simple superposition of known effects [5].

The decisive influence of the sign of coefficient *A* on flow asymmetry (Figs. 2–5) is explained by its physical meaning as the velocity gradient $\partial V_x/\partial y$ at the boundary. This gradient, specified at the upper wall, generates a transverse flow component throughout the entire volume due to viscous diffusion, leading to a shift in streamlines and vorticity maxima. Coefficient *B*,

governing the curvature of the profile ($\partial^2 V_x/\partial y^2$), determines the distribution of this transverse flow across the channel width, which is reflected in the change in the shape of the velocity isolines (Figs. 3, 4). The weakening of the effect of the boundary coefficients with distance from the upper wall (Fig. 5) is quantitatively described by the exponential dependences (13) and (14), which is consistent with the concept of disturbance damping from the boundary in a viscous fluid [16].

The dimensionless permeability parameter α depends on the dynamic viscosity μ ($\alpha = \rho V_w / \mu$). This explains the pronounced difference between the flow of water and petroleum (Figs. 6, 8).

For high-viscosity fluids (low α values), the solution far from the boundaries tends to a linear profile. However, the inhomogeneity in equation (8) for $U(z)$, caused by the term with B, leads to the concentration of shear in a thin near-wall layer, whose thickness is inversely proportional to $|\alpha|$. Thus, viscosity is not merely a multiplicative factor but a parameter governing the spatial localization of shear deformation. This has significant practical implications, for example, in calculating friction in bearings with porous lubrication [17].

The obtained solution is verified, as it correctly reproduces known limiting cases. For $\alpha \to 0$, it transforms into the solution for flow with a quadratic condition on an impermeable wall [18]. For $A, B \to 0$, it reduces to the classical exponential profile for permeable walls [19]. The simultaneous transition $\alpha, A, B \to 0$ yields the linear profile of classical Couette flow [2].

The explicit form of the solution allows for direct assessment of the effect of each parameter on the flow field, which is valuable for engineering design. For example, in a microfluidic mixer, the microrelief of the wall can be varied (via A and B) to generate a specific vortex structure that enhances mixing [20]. In the problem of porous bearing lubrication, the model enables an analytical connection between oil viscosity, seepage rate, and surface roughness (via A, B), and the distribution of shear stress and energy dissipation [21].

The basic limitation of the model is its assumptions of steady, laminar, and Newtonian flow behavior. Extending the model to account for turbulence is beyond the scope of this research. This represents a separate complex problem, requiring a transition to the Reynolds-averaged Navier-Stokes equations (RANS) or Large Eddy Simulation (LES) models. [20]. Another promising direction is generalization for non-Newtonian fluids [21] and unsteady regimes [22]. This would allow for the modeling of a wider class of applied problems, such as pulsating flows in biomedical devices.

Conclusion. For the first time, an exact analytical solution to the stationary Navier-Stokes equations has been obtained, describing generalized Couette flow of a Newtonian fluid between permeable plates with a quadratic velocity profile at the boundary.

The parametric analysis has revealed that the linear coefficient A of the boundary condition determines the direction of asymmetry in the velocity and vorticity fields, while the quadratic coefficient B determines the degree of their spatial nonlinearity.

Dynamic viscosity is shown to be a key parameter controlling the thickness of the shear layer. For high-viscosity media, the main velocity gradient is localized in a thin near-wall region, whereas for low-viscosity fluids, the velocity profile is close to linear across the entire channel height.

The results of this research provide an analytical foundation for solving applied problems in microfluidics, membrane technologies, and tribology, where flow control under conditions of boundary permeability and complex boundary conditions is required.

Further research is related to refining and expanding the model. In perspective, it could be extended to account for the non-Newtonian properties of the fluid, unsteady regimes, and flow stability.

References

1. Papanastasiou T, Georgios G, Alexandrou AN. *Viscous Fluid Flow*. Boca Raton FL: CRC Press; 2021. 434 p. https://doi.org/10.1201/9780367802424

2. Temam R. *Navier-Stokes Equations: Theory and Numerical Analysis*, 3rd rev. ed. Providence, RI: AMS; 2001. 500 p.

3. Ganie AH, Memon AA, Memon MA, Al-Bugami AM, Bhatti K, Khan I. Numerical Analysis of Laminar Flow and Heat Transfer through a Rectangular Channel Containing Perforated Plate at Different Angles. *Energy Reports*. 2022;8:539–550. https://doi.org/10.1016/j.egyr.2021.11.232

4. Vafai K. *Handbook of Porous Media.* Boca Raton, FL: CRC Press; 2015. 959 p. https://doi.org/10.1201/B18614

5. Wang FZ, Animasaun IL, Muhammad T, Okoya SS. Recent Advancements in Fluid Dynamics: Drag Reduction, Lift Generation, Computational Fluid Dynamics, Turbulence Modelling, and Multiphase Flow. *Arabian Journal for Science and Engineering*. 2024;49(8):10237–10249. https://doi.org/10.1007/s13369-024-08945-3

6. Almuthaybiri SS, Tisdell CC. Laminar Flow in Channels with Porous Walls: Advancing the Existence, Uniqueness and Approximation of Solutions via Fixed Point Approaches. *Journal of Fixed Point Theory and Applications*. 2022;24:55. https://doi.org/10.1007/s11784-022-00971-8

7. Shvarts KG. Plane-Parallel Adjective Flow in a Horizontal Incompressible Fluid Layer with an Internal Linear Heat Source. *Fluid Dynamics*. 2019;53(1):524-528.

8. Waqas H, Farooq U, Dong Liu, Abid M, Imran M, Muhammad T. Heat Transfer Analysis of Hybrid Nanofluid Flow with Thermal Radiation through a Stretching Sheet: A Comparative Study. *International Communications in Heat and Mass Transfer*. 2022;138:106303. https://doi.org/10.1016/j.icheatmasstransfer.2022.106303

9. Karmakar S, Usha R, Chattopadhyay G, Millet S, Ramana Reddy JV, Shukla P. Stability of a Plane Poiseuille Flow in a Channel Bounded by Anisotropic Porous Walls. *Physics of Fluids*. 2022;34(3):034111. https://doi.org/10.1063/5.0083217

10. Mirzaei A, Jalili P, Afifi MD, Jalili B, Ganji DD. Convection Heat Transfer of MHD Fluid Flow in the Circular Cavity with various obstacles: Finite element approach. *International Journal of Thermofluids*. 2023;20:100522. https://doi.org/10.1016/j.ijft.2023.100522

11. Gubareva KV, Eremin AV. Numerical Solution to the Problem of Thermal Conductivity in a Porous Plate with a Topology of Triply Periodic Minimal Surfaces. *Advanced Engineering Research* (*Rostov-on-Don*). 2025;25(1):23–31. https://doi.org/10.23947/2687-1653-2025-25-1-23-31

12. Goruleva LS, Prosviryakov EYu. Exact Solutions to the Navier-Stokes Equations for Describing Inhomogeneous Isobaric Vertical Vortex Fluid Flows in Regions with Permeable Boundaries. *Diagnostics*, *Resource and Mechanics of Materials and Structures*. 2023;1:41–53. https://doi.org/10.17804/2410-9908.2023.1.041-053

13. Polyanin AD, Zaitsev VF. *Handbook of Exact Solutions for Ordinary Differential Equations,* 2nd ed. Boca Raton, FL: CRC Press; 2003. 816 p.

14. Goruleva LS, Prosviryakov EYu. Unidirectional Steady-State Inhomogeneous Couette Flow with a Quadratic Velocity Profile Along a Horizontal Coordinate. *Diagnostics*, *Resource and Mechanics of Materials and Structures*. 2022;3:47–60. https://doi.org/10.17804/2410-9908.2022.3.047-060

15. Roache PJ. *Verification and Validation in Computational Science and Engineering.* Albuquerque, NM: Hermosa Publishers; 1998. 446 p.

16. Peiqing Liu. Boundary Layer Theory and Its Approximation. In book: *Aerodynamics*. New York, NY: Springer; 2022. P. 307–393 https://doi.org/10.1007/978-981-19-4586-1_6

17. Zhixiang Feng, Qingqing Ye. Turbulent Boundary Layer over Porous Media with Wall-Normal Permeability. *Physics of Fluids.* 2023;35(9):095111. https://doi.org/10.1063/5.0160773

18. Kulikovsky A. Laminar Flow in a PEM Fuel Cell Cathode Channel. *Journal of The Electrochemical Society.* 2023;170(2):024510. https://doi.org/10.1149/1945-7111/acba47

19. Nield DA, Bejan A. *Convection in Porous Media.* New York, NY: Springer; 2017. 640 p. https://doi.org/10.1007/978-3-319-49562-0

20. Pope SB. *Turbulent Flows.* Cambridge: Cambridge University Press; 2000. 807 p.

21. Das D, Mondal K, Poddar N, Ping Wang. Transient Dispersion of a Reactive Solute in an Oscillatory Couette Flow through an Anisotropic Porous Medium. *Physics of Fluids*. 2024;36(2):023610. https://doi.org/10.1063/5.0184921

22. Lemarie-Rieusset PG. *The Navier-Stokes Problem in the 21st Century*, 2nd ed. New York: Chapman and Hall/CRC; 2023. 778 p. https://doi.org/10.1201/9781003042594

About the Authors:

Kristina V. Gubareva, Cand.Sci. (Eng.), Associate Professor of the Department of Industrial Thermal Power Engineering, Samara State Technical University (244, Molodogvardeyskaya Str., Samara, 443100, Russian Federation), SPIN-code, ORCID, ScopusID, r.kristina2017@mail.ru

Evgenii Yu. Prosviryakov, Dr.Sci. (Phys.-Math.), Associate Professor of the Department of Information Technology and Control Systems, Ural Federal University (19, Mira Str., Ekaterinburg, 620002, Russian Federation), Head of the Nonlinear Vortex Hydrodynamics Sector, Institute of Engineering Science, RAS (Ural Branch) (34, Komsomolskaya Str., Ekaterinburg, 620049, Russian Federation), SPIN-code, ORCID, ScopusID, ResearcherID, evgen_pros@mail.ru

Anton V. Eremin, Dr.Sci. (Eng.), Associate Professor, Vice-Rector for Scientific Work, Head of the Department of Industrial Thermal Power Engineering, Samara State Technical University (244, Molodogvardeyskaya Str., Samara, 443100, Russian Federation), SPIN-code, ORCID, ScopusID, ResearcherID, a.v.eremin@list.ru

Claimed Contributorship:

KV Gubareva: investigation, software, writing – original draft preparation, visualization.
EYu Prosviryakov: conceptualization, data curation, methodology, writing – review & editing.
AV Eremin: formal analysis, validation, writing – review & editing.

Conflict of Interest Statement: **the authors declare no conflict of interest.**

All authors have read and approved the final manuscript.

Об авторах:

Кристина Владимировна Губарева, кандидат технических наук, доцент кафедры «Промышленная теплоэнергетика» Самарского государственного технического университета (443100, Российская Федерация, г. Самара, ул. Молодогвардейская, 244), SPIN-код, ORCID, ScopusID, r.kristina2017@mail.ru

Евгений Юрьевич Просвиряков, доктор физико-математических наук, доцент, профессор кафедры «Информационные технологии и системы управления» Уральского федерального университета имени первого Президента России Б.Н. Ельцина (620062, Российская Федерация, г. Екатеринбург, ул. Мира, 19), заведующий сектором нелинейной вихревой гидродинамики Института машиноведения имени Э.С. Горкунова Уральского отделения Российской академии наук (620049, Российская Федерация, г. Екатеринбург, ул. Комсомольская, 34), SPIN-код, ORCID, ScopusID, ResearcherID, evgen_pros@mail.ru

Антон Владимирович Еремин, доктор технических наук, доцент, проректор по научной работе, заведующий кафедрой «Промышленная теплоэнергетика» Самарского государственного технического университета (443100, г. Самара, ул. Молодогвардейская, 244). SPIN-код, ORCID, ScopusID, ResearcherID, a.v.eremin@list.ru

Заявленный вклад авторов:

К.В. Губарева: проведение исследования, разработка программного обеспечения, написание черновика рукописи, визуализация.

Е.Ю. Просвиряков: разработка концепции, курирование данных, разработка методологии, написание рукописи — внесение замечаний и исправлений.

А.В. Еремин: формальный анализ, валидация результатов, написание рукописи — внесение замечаний и исправлений.

Конфликт интересов: **авторы заявляют об отсутствии конфликта интересов.**

Все авторы прочитали и одобрили окончательный вариант рукописи.

Received / **Поступила в редакцию** 04.12.2025
Reviewed / Поступила после рецензирования 22.12.2025
Accepted / **Принята к публикации** 14.01.2026